

Behaviour of slender concrete-filled dual steel tubular columns subjected to eccentric loads

V. Albero^a, C. Ibañez^{b*}, A. Piquer^a, D. Hernández-Figueirido^a

*^aDepartment of Mechanical Engineering and Construction, Universitat Jaume I,
Castellón, Spain*

*^bDepartment of Construction Engineering and Civil Engineering Projects, Universitat
Politécnica de València, Valencia, Spain*

** Corresponding author: caribus@upv.es*

ABSTRACT

In this paper an experimental program on concrete-filled steel tubular columns subjected to eccentric loads is presented. The columns have different cross-sectional configurations, including single concrete-filled steel tubular columns (CFST) and concrete-filled dual steel tubular columns (CFDST). The response of all the columns was studied and the physical state of all the specimens after the tests was checked. The level of utilisation achieved by each type of column in relation to its cross-sectional resistance was analysed together with the influence of the extra inner tube or the inner filling of concrete for the CFDST specimens. Finally, EN1994-1-1 provisions were assessed by comparing the experimental results with the predictions given by the simplified method which appears to be conservative in this case.

Keywords: Slender columns, load eccentricity, double-tube, double-skin, concrete-filled steel tubular columns, Eurocode 4.

1 INTRODUCTION

Based on the benefits of concrete-filled steel tubular (CFST) columns, an innovative section formed by two steel tubes placed concentrically and concrete filling the hole between them and the inner tube appeared. It allows to enhance the advantages of CFST columns in their main applications which involve supporting high compression loads, for example when are used in high-rise buildings, electricity transmission towers or bridge piers. This new cross-section known as CFDST (concrete-filled dual skin tubular columns) can be divided into two categories of cross-sections as shown in Fig. 1: double-skin sections (Fig. 1a), where the inner steel tube is empty, and double-tube sections (Fig. 1b), where it is filled with concrete.

For the same load capacity, CFDST columns keep the excellent properties of single CFST columns (such as high bearing resistance, durability, inherent good fire behaviour and good constructability) but, in addition, due to their configuration with two tubes, CFDST allow to reduce the weight and increase bending stiffness. Clearly, the use of this type of dual sections leads to a reduction of concrete cost and in general, construction costs [1]-[13].

There are different possibilities to build CFDST columns combining tubes with different shapes (circular, square, rectangular). However, in general, those formed by circular columns have proved to be the most efficient in bearing the same ultimate load that columns with the same steel cross-sectional area of other typologies.

Most of the works to date performed with the aim of characterizing CFDST cross-sections have focused on double-skin stub columns with normal strength concrete. With regard to double-tube columns, it is worthy to mention the work by Liew and Xiong [14] on circular-circular CFDST columns where the experimental results were also contrasted with EN1994-1-1 (EC4) [15] predictions which were conservative. However, once again, all were stub columns so the second-order effects could not be analysed.

In fact, the number of experimental programs on slender CFDST column is still scarce in comparison with those that focused on stub columns. In this line, it should be highlighted the research carried out by Essopjee and Dundu [16] who tested 32 double-skin specimens under compression loads and proposed a new buckling curve for the European code. Also, the work by Wan and Zha [17] presented results from tests on slender double-tube columns. Nevertheless, in both programs the columns were axially loaded, without eccentricity.

More recently, in the works presented by Romero et al. [18], [19] and Ibáñez et al. [20], the results of a series of tests on slender CFDST columns subjected to concentric and eccentric compression loads were discussed. Even though the number of specimens analysed in these publications was limited some trends were detected. Although under compression loads the effectiveness of CFDST columns is higher than the equivalent single CFST columns, under eccentric loads this phenomenon was not observed. Besides, the results from the eccentric specimens were compared with the EC4 [15] predictions, which were slightly insecure.

Considering the literature review presented above, it is clear the lack of experimental works on slender CFST columns under eccentric loads that allows to properly understand their behaviour in this situation. Also, efforts are being made in developing numerical models to simulate the behaviour of eccentrically loaded CFDST columns considering geometric and material nonlinearities, as evidenced by recently published works [21][22]. Generating a rich database of tests results on this type of columns will also permit a proper assessment of the current codes, the validation of numerical models and the proposal of new simplified models.

Therefore, in this paper, a short program on CFST columns subjected to eccentric loads is presented. The experimental data is analysed and the behaviour of the different columns is compared. A numerical model is employed to calculate the EC4 predictions which are compared with the tests results. This is the beginning of an experimental program where, in the

future, also slender CFDST columns are tested with eccentricities of different values at their ends.

2 EXPERIMENTAL PROGRAM

2.1 Specimens analysed

In this paper, the results of a series of four tests on composite columns subjected to eccentric loads are presented. The program consists of two CFDST specimens, with double-skin (DS) and double-tube (DT) configuration respectively, and the corresponding single CFST columns (CFSTO and CFSTI). The former two were also tested as reference to assess the synergy of combining two tubes. The list of specimens is shown in Table 1

In the CFDST columns tested, both the inner and the outer tube are circular steel hollow sections, as those shown in Fig. 1. All the outer and inner steel tubes had the same dimensions as shown in Table 1. The single specimen CFSTO had the same outer diameter as the outer steel tube of the double ones. On the other hand, the specimen CFSTI was made with the steel tube used as inner tube in the double specimens. In this program, all the columns had a nominal length of 3000 mm and were subjected to loads with an eccentricity of 50 mm applied at both ends.

To characterise the cross-section, the hollow section ratio (ψ) can be used in concrete-filled dual steel columns. This parameter gives information about the size of the ring cavity that exists between the steel tubes and is calculated as the ratio between the outer diameter of the inner steel tube (D_i) and the inner diameter of the outer steel tube ($D_o - 2t_o$):

$$\psi = \frac{D_i}{D_o - 2t_o} \quad (1)$$

A value of ψ equal to 0 corresponds to a single CFST column. In this case, the value of ψ for DS and DT specimens is 0.51 as shown in Table 1 which is in accordance to the guidelines given by Han et al. [23] for the design of this type of column where the value of ψ is recommended to be between 0 and 0.75.

2.2 Material properties

Steel tubes

For these tests, all steel tubes were cold-formed carbon steel and supplied by the same manufacturer. The steel grade of the tubes varied between S355 and S275. For all the hollow steel tubes employed, the actual values of the yield strength ($f_{y,o}$, $f_{y,i}$) were determined through the corresponding coupon tests and are summarised in Table 1. For the corresponding calculations, and according to the European standards, the modulus of elasticity of steel was set to 210 GPa.

Concrete

For all the specimens, concrete with a nominal compressive strength of C30 was employed. The concrete was delivered already mixed by an external supplier and was carefully pumped into the columns. In order to guarantee the proper filling of both the steel tubes and the molds for the samples, the concrete was gradually pour in several layers and each layer was compacted by means of a vibrator rod. Later, the composite columns were covered with wet clothes and let to cure. To characterize the concrete with its actual compressive strength, a set of 3 concrete samples was also prepared and cured in standard conditions. Subsequently, the same day of the experiments on the columns, the corresponding tests were carried out on the 150x300 mm cylinders. In the DT specimen, the same concrete was used to fill both the inner

steel tube and the ring between the two tubes. The actual value of the compressive strength of the concrete ($f_{c,o}$, $f_{c,i}$) is shown in Table 1.

2.3 Test setup

All the columns were manufactured and tested at Universitat Jaume I in Castellón (Spain). In Fig. 2 and Fig. 3 a general view of the specimens preparation and collocation can be seen together with a schematic of the test setup and some details. For the experiments, a horizontal testing frame with capacity of 5000 kN was used. Fig. 2a shows one of the specimens prepared for the experiments. A 1m grid was painted at mid-height of the columns to facilitate the visualization of the deformed shape of the column, Fig. 2b.

In each column, a steel plate with dimensions 300x300x10 mm was welded at both ends (Fig. 2b). These steel plates were screwed to a rigid plate through four M12 bolts placed at the plate corners. The knife form of the rigid plate allows to apply the load with eccentricity without any rotational restraint, Fig. 2b. Thus, it can be considered that all the specimens were tested under pinned-pinned (P-P) end conditions, resulting columns with a buckling length of 3000 mm. The columns straightness was measured just before the test and no appreciable imperfection was observed.

To guarantee the accuracy of the measurements and in order to measure the post-peak column behaviour, the corresponding displacement control test was conducted after the correct collocation of the column (Fig. 2c). The displacement control was configured to move forward the load device with a displacement velocity of 1 mm/min.

As mentioned in the previous section, the load was applied with the same eccentricity at both ends with a value of 50 mm. Linear variable displacement transducers (LVDTs) were

placed at five points along the column (0.25L, 0.375L, 0.5L, 0.625L and 0.75L, being L the length of the column) with the aim of measuring the deflection, see Fig. 3a.

At the central cross-section of the columns, strains were measured by means of six electrical strain gauges placed at the outer steel tube which recorded the deformation in the longitudinal and transversal directions at three locations: location 1 at 0°, location 2 at 90° and location 3 at 180° according to the detail shown in Fig. 3b.

To initialise the tests from a neutral position, and so that the self-weight of the columns did not cause initial deflections due to the horizontal loading arrangement, two vertical supports were positioned below the columns before loading.

3 TEST RESULTS

3.1 Force-displacement results

As it was described in the previous section, the test was carried out using a displacement control procedure which consisted of the application of an imposed displacement with a constant velocity of 1 mm/min. The specimens were tested to failure and after the peak load was achieved, the experiment continued at least until the load reached back the 85% of its peak load in order to obtain enough experimental data for the subsequent analysis. The behaviour of the specimens was generally ductile so the tests were conducted in a gentle and controlled way. Once the experiment was finished, the specimen was removed and kept for the posterior examination.

One of the most representative results that can be obtained from these tests is the response in terms of load versus deflection at mid-height of the column which was registered during the tests by means of the corresponding LVDT. In Fig. 4a these curves are plotted for all the specimens.

In Fig. 4a a similar peak value of around 900 kN can be observed for the DS, DT and CFSTO columns while, for CFSTI, the maximum axial force resulted around 100.6 kN. This figure also shows the post-peak behaviour for each specimen. As mentioned above, each test was stopped only when the axial force dropped by 15% of the maximum axial force. The maximum mid-height displacement showed by the specimens was around 60 mm for specimens DS, DT and CFSTO, whereas specimen CFSTI reached more than 100 mm. The exact values of the maximum axial load (N_{exp}), the axial load at the end of the test (N_{end}), and their associated displacements (Δ_N, Δ_{end}) are also displayed in Table 2.

As shown in Table 1, the actual yield strength ($f_{y,o}, f_{y,i}$) was not the same for all the steel tubes. This resulted in difficulty analysing the curves expressed in terms of the absolute axial load. Therefore, in Fig. 4b, the same curves are expressed in relative terms by means of the level of utilisation (n) with respect to the plastic axial resistance of the cross-section ($N_{pl,Rd}$) calculated as follows:

$$N_{pl,Rd} = A_{s,i}f_{y,i} + A_{s,o}f_{y,o} + A_{c,i}f_{c,i} + A_{c,o}f_{c,o} \quad (1)$$

where $A_{s,i}$ and $A_{s,o}$ are the cross-sectional areas of the inner and outer steel tubes in mm² respectively; $A_{c,i}$ and $A_{c,o}$ are the inner and outer concrete cross-sectional areas in mm²; and $f_{y,i}$, $f_{y,o}$, $f_{c,i}$ and $f_{c,o}$ are expressed in MPa as in Table 1.

In Fig. 4b, it can be clearly seen that specimen DS reaches the highest level of utilisation during the tests followed by DT and CFSTO. Specimen CFSTI has the lowest level of utilisation. For all of the columns, the values of the relative slenderness ($\bar{\lambda}$) are summarised in Table 1. The higher the slenderness, the lower the level of utilisation. For specimens CFSTO and DT the curves are very similar and follow the exact same path in the pre-peak region. When the second-order effects are higher, the influence of the inner steel tube allows column DT to

work in a more ductile manner thus increasing the load level achieved. The maximum values of the level of utilisation (n_{exp}) are summarised in Table 2.

The curve for specimen DS is much higher than the DT curve. Filling the inner tube with concrete increases the modulus of inertia and the cross-sectional area of the column. However, the beneficial effect in the increased modulus of inertia does not compensate the increment in the area and, therefore, the radius of gyration is, in this case, smaller for DT than for DS. Subjected to eccentric loads, the lower slenderness of DS delays the appearance of second-order effects which, in turn, allows the column to achieve a higher level of utilisation.

3.2 Failure mode

The failure mode for all of the specimens was buckling. In Fig. 6 the deformed shape of the columns after the test is shown. The buckled shape follows approximately a sinusoidal curve. The deflection of the columns at different moments of the experiment is displayed in Fig. 6: 1) Deflection at peak load; 2) Deflection at the end of the test; 3) Deflection after recovery (permanent). For these moments, the values of the deflection at mid-height are summarised in Table 2. Specimen CFSTI had the highest deflection values and the complete deformed shape at the end of the test could not be recorded since the displacement at mid-height was too high for the measuring capacity of the LVDTs. The other three specimens had similar values of deflection both at peak load and after recovery.

To analyse the state of the columns after the tests, part of the outer steel tube was cut in order to leave the inner concrete exposed. In the CFDST specimens, the concrete in the outer ring was removed to access the inner steel tube. This procedure is shown in Fig. 7 for specimen DS. As expected, tension cracks appeared in the concrete on the tension side. On the contrary, some cracks due to the crushing of the concrete were observed in the opposite side together

with a soft yielding of the outer steel tube in the area of the cracks. No local buckling was observed in the inner steel tube.

In Fig. 8 and Fig. 9, the longitudinal and transversal strains measured at mid-height in the outer steel tube in all of the columns are shown. Three different points of the cross-section at mid-height were monitored: point 1 at 0° (L1 and T1), point 2 at 90° (L2 and T2) and point 3 at 180° (L3 and T3), as shown in Fig. 3b. Data from point 1 are displayed with a solid line, point 2 with a dashed line and point 3 with a dotted line. In the same way, for the sake of clarity, the colour of the lines changed gradually from light grey for CFSTI to black for DT.

For the longitudinal strain in Fig. 8, the values of both the tension and the compression strains measured by L1 and L3 respectively are within the same order of magnitude for CFSTO, DS and DT. L2, the gauge located at the mid-section axis, also measured compression strains although lower than those from L3, which means that the neutral axis moved to the top of the section, being bigger the part of the cross-section working in compression. This can also be observed in Fig. 10 where, for the cross-section at mid-height, the plane of deformation at peak load has been displayed for all the specimens. In Fig. 10 can be seen that for specimen CFSTI the neutral axis is very close to the centre of the section, indicating that this column is working practically under pure bending. This is in accordance to what can be observed in Fig. 8, where it can be seen that the strains registered for specimen CFSTI are much lower. Also, the change of sign in the strain L2 indicates the premature loss of stability of the column.

Transversal strains in T1 and T3 were tension and compression strains respectively, Fig. 9. Strains measured by T2 were also tension strains. Specimen CFSTI had the lowest strain values and the other three specimens had strains of a similar order of magnitude but in all cases lower than the longitudinal strains.

Fig. 11 shows the evolution of the longitudinal strain, $L3$, versus the transversal strain, $T3$, for the gauge placed in the compression side of the column. As can be observed, no sudden changes occur in the graph which corroborates the fact that no local buckling was observed in the outer tube. At the beginning of the graph almost the same linear relationship is detected for all the columns with a mean value for the slope of 0.29 (see the enlarged graph on the bottom left of Fig. 11), which matches Poisson's ratio. When the steel yields, the slope changes and the response depends on the type of column.

An additional interesting result from the experiments can be observed in the moment – curvature behaviour of each specimen. The curvature (χ_y) of the column cross-section at mid-height can be directly obtained from the longitudinal strain at points 1 (ε_{L1}) and 3 (ε_{L3}) as follows:

$$\chi_y = \frac{\varepsilon_{L1} - \varepsilon_{L3}}{D_o} \quad (2)$$

In turn, the value of the bending moment can be easily deduced from the load registered during the experiment (N) and the load eccentricity (e):

$$M_z = N \cdot e \quad (3)$$

Fig. 12 shows the $M_z - \chi_y$ curve for each experiment. As in previous results, double-tube and double-skin tubes present similar behaviour to CFSTO while CFSTI behaves in a very different manner due to its high slenderness. Moreover, it is well known that the slope of the $M_z - \chi_y$ curve represents the column flexural stiffness. These curves may be used to compare the stiffness of each specimen. It should be noted that EN 1994-1-1 [15] Clause 6.7.3.4 provides an expression for the determination of the effective flexural stiffness in slender members. This expression for unreinforced CFST columns is as follows:

$$(EI)_{eff,II} = K_0 \cdot (E_{a,o} I_{a,o} + E_{a,i} I_{a,i} + K_{c,II} E_{cm,o} I_{c,o} + K_{c,II} E_{cm,i} I_{c,i}) \quad (4)$$

where $E_{a,o}$ and $E_{a,i}$ are the modulus of elasticity of outer and inner steel tubes respectively; $E_{cm,o}$ and $E_{cm,i}$ are the secant modulus of elasticity of the outer and inner concrete; $I_{a,o}$ and $I_{a,i}$ are the modulus of inertia of outer and inner steel tubes sections; $I_{c,o}$ and $I_{c,i}$ are the modulus of inertia of the outer and inner concrete section respectively; and K_0 and $K_{c,II}$ are the calibration and correction factors respectively that adopt the next values $K_0 = 0.9$ and $K_{c,II} = 0.5$.

Fig. 13 details the elastic range of each $M_z - \chi_y$ curves and contrasts them with the value given by EC4 [15] (red line). This comparison shows good agreement in the elastic range for each specimen, however, the real flexural stiffness of each column drops substantially for higher loads due to plasticity and second-order effects. This behaviour is however not captured by the code because second-order effects are introduced in the EC4 [15] method using a different approach which will be described in section 4.

3.3 Ductility index

In Fig. 14a the level of utilisation-axial shortening curves are shown for all the columns. It can be observed that the trend followed by the curves is similar to the one observed for the deflection at mid-height analysed in section 3.2. Based on these curves, the ductility index (DI) is obtained as the inverse ratio between the axial shortening (δ_N), at the peak load (n_{exp}), and the axial shortening ($\delta_{85\%}$), after the peak load has been achieved and has fallen by 15% ($n_{85\%}$). In this work, the definition proposed by Han et al. [24] is adopted:

$$DI = \frac{\delta_{85\%}}{\delta_N} \quad (5)$$

Fig. 14b details how the values required in Eq. (5) can be extracted from the graph for specimen DS. The DI calculated values for the specimens tested are summarised in Table 3 together with the values of δ_N , $\delta_{85\%}$ and $n_{85\%}$. The higher the value of DI, the higher the ductility

of the column as this implies that the slope of the post-peak curve is softer. Thus, the most slender column, CFSTI, shows in this case the highest DI, whereas the other three specimens had DI lower values of a similar magnitude.

3.4 Concrete-steel contribution ratio (CSCR)

The effect of placing an inner steel tube and an extra filling of concrete in the cross-sectional configuration is analysed by means of the mechanical contribution of the different components. A mechanical ratio defined as the concrete-steel contribution ratio (CSCR) by some of the authors in previous works [19][20] is also employed in this case. The CSCR is calculated as the ratio between the maximum level of utilisation achieved by the CFDST (n_{exp}) and the maximum level of utilisation measured for the simple column ($n_{exp,CFSTO}$).

$$CSCR = \frac{n_{exp}}{n_{exp,CFSTO}} \quad (6)$$

A value less than unity indicates that the new configuration does not improve the load bearing capacity of the CFSTO column. The calculated values are shown in Table 3. For the DS specimen, the CSCR is 1.25 which means that the inner steel tube added to the section improves the level of utilisation of the column by 25% when subjected to eccentric loads. For the DT specimen, however, CSCR is only 1.08, with an improvement of only the 8% in the level of utilisation. As can be seen, the information given by this parameter is in concordance with the trend observed previously through the analysis of the level of utilisation-deflection curves. As analysed above, given the different cross-sectional properties of the columns, the relative slenderness changes for the same buckling length.

3.5 Inner concrete contribution ratio (ICCR)

Finally, the variation in the level of utilisation of the double-skin column (DS) when the inner steel tube is filled with concrete and becomes a double-tube column (DT) is evaluated by means of the inner concrete contribution ratio (ICCR). Again, according to previous works published by some of the authors [19][20], it is obtained as the ratio between the maximum level of utilisation measured for the DT column and the DS specimen. A value more than unity indicates that filling the inner tube with concrete is beneficial.

$$ICCR = \frac{n_{exp,DT}}{n_{exp,DS}} \quad (7)$$

In this case, the value of ICCR obtained when comparing column DT and DS is 0.87 which indicates that, in this case, and under the load conditions of the experimental program, filling the inner steel tube reduces the level of utilisation of the column by 13%. This observation agrees with the behaviour observed when Fig. 4b was analysed. Column DT is, in this case, more slender than DS which leads to a poorer response when second-order effects appear not allowing the specimen to reach a higher level of utilisation.

4 ASSESSMENT OF EN1994-1-1 PREDICTIONS

The experimental results described above were compared with the maximum load obtained through the European standard EN 1994-1-1[15]. Specifically, Clause 6.7.3, a simplified method from EC4 for composite columns or composite compression members is applied hereafter.

For combined compression and uniaxial bending, Clause 6.7.3.6 (1) from EC4 provides the following expression:

$$\frac{M_{Ed}}{M_{pl,N,Rd}} \leq \alpha_M \quad (8)$$

where M_{Ed} is the greatest bending moment within the column length which includes the column imperfection effect and second-order moment; and $M_{pl,N,Rd}$ represents the plastic bending moment resistance taking into account the applied axial force N_{Ed} . The coefficient α_M is 0.9 for steel grades lower or equal than S355 and 0.8 for steel grades higher than S420. In the cases studied in this work, only specimen CFSTO was calculated with $\alpha_M = 0.8$ (see steel yield strengths in Table 1).

Additionally, the plastic bending moment calculation for each axial load ($M_{pl,N,Rd}$) requires the analysis of the interaction between compression and uniaxial bending. In this work, instead of using the simplified proposal from EC4 Clause 6.7.3.2(5), a cross-section cell discretization method is used to perform the bending equilibrium equations, see Fig. 15.

The column cross-section is discretized in a triangular mesh with a maximum cell size of 3 mm. Each cell is characterized by its area, position and its corresponding material properties. The non-linear stress-strain behaviour for concrete and steel from EN 1994-1-1 [15] are assumed. The Navier-Bernoulli assumption is adopted, which states that a plane cross-section remains plane after bending. Thus, the linear strain distribution can be derived from each curvature (χ_y) of the cross-section. Then, the stress-strain material constitutive models can be used to obtain the stress state of each cell. Besides, for a given applied load, the neutral axis position and the strain of the reference point (ε_0) can be determined based on the force balance equation:

$$\sum_{i=1}^n A_i \sigma_i - N_{Ed} = 0 \quad (9)$$

where A_i and σ_i are respectively the area and stress of cell i ; and N_{Ed} is the applied force.

Afterwards, the bending capacity of the cross-section can be obtained by solving Eq. (10).

By iteratively increasing the curvature, the M_z - χ_y curve can be generated.

$$\sum_{i=1}^n A_i \sigma_i y_i - M_z = 0 \quad (10)$$

where y_i is the y-axis position of the centroid of cell i ; and M_z is the bending capacity.

The M_z - N interaction curve is computed by solving Eq. (6) and (7) repetitively using different axial load levels from 0 to $N_{pl,Rd}$. Moreover, it should be noticed here that following EC4 [15]. The cross-sectional axial plastic resistance ($N_{pl,Rd}$) was calculated without taking account of any increase in the concrete compressive strength caused by confinement since the load eccentricity is higher than 0.1 ($e/D > 0.1$) and the relative slenderness is higher than 0.5 ($\bar{\lambda} > 0.5$) for all of the tested specimens.

Once the M_z - N interaction curve has been built, the member imperfection and second-order effects should also be added to consider the member slenderness. In this case, the amplification factor method from EN1994-1-1 [15] Clause 6.7.3.4(5) is used, where second-order effects may be taken into account by multiplying the first-order bending moment by a factor k :

$$k = \frac{\beta}{1 - \frac{N_{Ed}}{N_{cr,eff}}} \quad (11)$$

where $N_{cr,eff}$ is the critical normal force corresponding to the effective flexural stiffness with the effective length taken as the column length; and β is the equivalent moment factor given by EN 1994-1-1 [15] Table 6.4 which depends on the bending moment distribution (linear or parabolic) and the end moment ratio r :

$$\beta = 0.66 + 0.44r \geq 0.44 \quad (12)$$

Note that the test setup was configured with the same load eccentricity at both ends of the column. Thus the bending moment remains constant within the whole column length and the end moment ratio takes a value of $r=1.0$. Therefore, the equivalent moment factor β for these specimens is equal to 1.1.

In addition, a member imperfection of $L/300$ according to EN 1994-1-1 [15] Table 6.5 is also considered. This imperfection works as an additional load eccentricity but using an amplification factor k equal to 1.0 as suggested by EN 1994-1-1 [15] Table 6.4.

It should be noted that, as can be seen in Eq. (11), the amplification factor depends on the applied axial force (N_{Ed}). An iterative process is therefore required to compute the impact of the second-order effects on the bending moment. 0 shows the $\alpha_M M_z-N$ interaction curve for each specimen with a bold solid black line; the first-order linear bending moment curve is a dashed blue line; and the bending moment curve including the amplification factor (k) of second-order effects and imperfection ($L/300$) is a solid blue line. The intersection between the $\alpha_M M_z-N$ interaction curve and the bending moment curve including the second-order effects (solid blue line) gives the failure load ($N_{b,Rd}$) prediction (blue point) of the method. For each column, the value of $N_{b,Rd}$ is also displayed in Table 4, column *EC4*. It should also be noted that the safety factor α_M is applied on each M_z-N interaction curve by an x-scaling of the interaction curve.

In addition, 0 also shows the experimental M_z-N interaction curve obtained from each test which is plotted in a solid red line. The maximum axial load achieved during the experiment (red point) represents the real failure load (N_{exp}) which is also presented in Table 4.

Regarding the EN 1194-1-1 [15] simplified method for composite columns, it should be highlighted that the member imperfection and the α_M coefficient have a remarkable effect on the accuracy of the prediction. However, current steel tube manufacturing processes may no

longer justify the application of the somewhat high member imperfection suggested by EC4 [15] Table 6.5. Thus, in order to assess the influence of these variables, two more values have been calculated: EC4*¹ is the predicted failure load when the member imperfection is not considered; and EC4*² is the predicted failure load when both the member imperfection and the α_M coefficient are dismissed ($\alpha_M=1$). These values are shown in Table 4.

For the three scenarios, the predicted failure load has been calculated (referenced above as EC4, EC4*¹ and EC4*²), the error in contrast with the experimental failure load is obtained for each specimen and presented in Table 4 and Fig. 17. The prediction error was measured as follows:

$$\xi = \frac{N_{exp}}{N_{b,Rd}} \quad (13)$$

For the EC4 prediction, the mean error is 1.09, lying on the safe side, and the standard deviation is 0.09. It can be seen that the influence of the member imperfection and the α_M coefficient on the EN 1194-1-1 method is high because the EC4*¹ and EC4*² predictions, which do not take account of these factors, result in less conservative (sometimes unsafe) results. This is an important point which warrants further investigation because the level of current manufacturing standards is relatively high when compared to the level of imprecision that the recommended values imply. Questions can then be asked of this method if the imperfections, which in reality are small these days, are relied upon to obtain conservative results. It suggests that there are certain physical phenomena that are not fully accounted for in the method.

Finally, it should be also noted from Fig. 17 that double-tube and double-skin EC4 method predictions are safer than those for simple CFST specimens. Therefore, although the number of experiments carried out is not enough to obtain consistent conclusions, these first results may indicate that EN1994-1-1 [15] provisions for combined compression and axial

bending are accurate enough to be used for double-tube and double-skin concrete filled steel tubular columns.

5 CONCLUDING REMARKS

In this paper, an experimental program on concrete-filled steel tubular columns with several cross-sectional configurations subjected to eccentric loads was described and the results obtained were presented and analysed. The EN1994-1-1 method used to predict the resistance of these columns was assessed. According to the results obtained using this model, the following conclusions can be drawn:

- There is a lack of experimental studies on CFST columns subjected to eccentric loads and, particularly, with different eccentricities at the ends. The authors really consider that more tests in this line should be done and, in fact, the continuation of the program presented here will include specimens with this type of loading.
- The failure mode observed for all of the specimens was global buckling, with a smooth post-peak branch in the load-deflection curves. The CFSTI specimen had the smoothest curve and the highest ductility index.
- Specimen DS had the highest level of utilisation subjected to eccentric loads. It was observed that the higher the slenderness, the lower the level of utilisation.
- The level of utilisation of specimen DS improved by 25% when compared to the single CFSTO. The level of DT only increased by 8%. The lower slenderness of DS delayed the appearance of second-order effects and allowed the column to work longer thus achieving

a higher level of utilisation. In the conditions of this experimental program, the DT column is less effective than the DS (13% less).

- The stiffness of the columns matches the value of the flexural stiffness given by the EN1994-1-1 formula in the initial stage of the curve, where the response is still linear. The values differ for higher loads.
- The simplified method from EN1994-1-1 gave conservative predictions with a low standard deviation for the CFDST columns analysed. Although the low number of tests was not sufficient to draw consistent conclusions, a conservative tendency was observed. Considering a coefficient for the member imperfection is crucial for the conservativeness of the method but, owing to the current manufacturing processes, the recommended value of this variable makes an unrealistic assumption of the imperfection.

ACKNOWLEDGEMENTS

The authors would like to express their sincere gratitude to Universitat Jaume I for the funding provided through the project UJI-B2018-58.

DATA AVAILABILITY

The processed data required to reproduce these findings cannot be shared at this time as the data also forms part of an ongoing study.

REFERENCES

- [1] Zhao XL, Grzebieta R. Strength and ductility of concrete filled double skin (SHS inner and SHS outer) tubes. *Thin-Walled Structures* 2002; 40: 199-213.
- [2] Elchalakani M, Zhao XL; Grzebieta R. Tests on concrete filled double-skin (CHS outer and SHS inner) composite short columns under axial compression. *Thin-walled Structures* 2002; 40 (5): 415-441.
- [3] Tao Z, Han LH, Zhao XL. Behaviour of concrete-filled double skin (CHS inner and CHS outer) steel tubular stub columns and beam-columns. *Journal of Constructional Steel Research* 2004; 60: 1129-1158.
- [4] Han LH, Tao Z, Huang H, Zhao XL. Concrete-filled double skin (SHS outer and CHS inner) steel tubular beam-columns. *Thin-Walled Structures* 2004; 42: 1329-1355.
- [5] Tao Z, Han LH. Behaviour of concrete-filled double skin rectangular steel tubular beam-columns. *Journal of Constructional Steel Research* 2006; 62(70): 631–646.
- [6] Zhao X, Han L. Double skin composite construction. *Progress in structural engineering and materials* 2006; 8 (3): 93-102.
- [7] Uenaka K, Kitoh H, Sonoda K. Concrete filled double skin circular stub columns under compression. *Thin-Walled Structures* 2010; 48 (1): 19-24.
- [8] Uenaka K, Kitoh H. Mechanical behavior of concrete filled double skin tubular circular deep beams. *Thin-Walled Structures* 2010; 49 (2): 256-263.
- [9] Yang YF, Han LH, Sun BH. Experimental behaviour of partially loaded concrete filled double-skin steel tube (CFDST) sections. *Journal of Constructional Steel Research* 2012; 71: 63-73.
- [10] Li W, Han LH, Zhao XL. Axial strength of concrete-filled double skin steel tubular (CFDST) columns with preload on steel tubes. *Thin-Walled Structures* 2012; 56: 9–20.

- [11] Li W, Ren QX, Han LH, Zhao XL. Behaviour of tapered concrete-filled double skin steel tubular (CFDST) stub columns. *Thin-Walled Structures* 2012; 57: 37–48.
- [12] Yuan YB, Yang JJ. Experimental and numerical studies of short concrete-filled double skin composite tube columns under axially compressive loads. *Journal of Constructional Steel Research* 2013; 80: 23-31.
- [13] Han LH, Li YJ, Liao FY. Concrete-filled double skin steel tubular (CFDST) columns subjected to long-term sustained loading. *Thin-Walled Structures* 2011; 49(12): 1534–1543.
- [14] Liew JYR, Xiong DX. Experimental investigation on tubular columns infilled with ultrahigh strength concrete. *Tubular Structures XIII* 2011; 1: 637-645.
- [15] CEN. EN 1994-1-1, Eurocode 4: Design of composite steel and concrete structures. Part 1-1: General rules and rules for buildings. Brussels, Belgium: Comité Européen de Normalisation; 2004.
- [16] Essopjee Y, Dundu M. Performance of concrete-filled double-skin circular tubes in compression. *Composite Structures* 2015; 133: 1276-1283.
- [17] Wan CY, Zha XX. Nonlinear analysis and design of concrete-filled dual steel tubular columns under axial loading. *Steel and Composite Structures* 2016; 20(3): 571-597.
- [18] Romero ML, Espinos A, Portolés JM, Hospitaler A, Ibáñez C. Slender double-tube ultrahigh strength concrete-filled tubular columns under ambient temperature and fire. *Engineering Structures* 2015; 99: 536–545.
- [19] Romero ML, Ibáñez C, Espinos A, Portolés JM, Hospitaler A. Influence of ultra-high strength concrete on circular concrete-filled dual steel columns. *Structures* 2017; 9: 13-20.
- [20] Ibáñez C, Romero ML, Espinos A, Portolés JM, Albero V. Ultra-high Strength Concrete on Eccentrically Loaded Slender Circular Concrete-filled Dual Steel Columns. *Structures* 2017; 12: 64-74.
- [21] Ahmed M., Liang QQ, Patel VI, Hadi MNS. Computational simulation of eccentrically loaded circular thin-walled concrete-filled double steel tubular slender columns. *Engineering Structures* 2020; 213: 110571.
- [22] Liang QQ. Numerical simulation of high strength circular double-skin concrete-filled steel tubular slender columns. *Engineering Structures* 2018, 168: 205-217.
- [23] Han LH, Lam D, Nethercot DA. *Design Guide for Concrete-filled Double Skin Steel Tubular Structures*. CRC Press; 2018.
- [24] Han LH, Zhao XL, Tao Z. Tests and mechanics model for concrete filled SHS stub columns, columns and beam-columns. *Steel & Composite Structures – An International Journal* 2001; 1(1): 51-74.

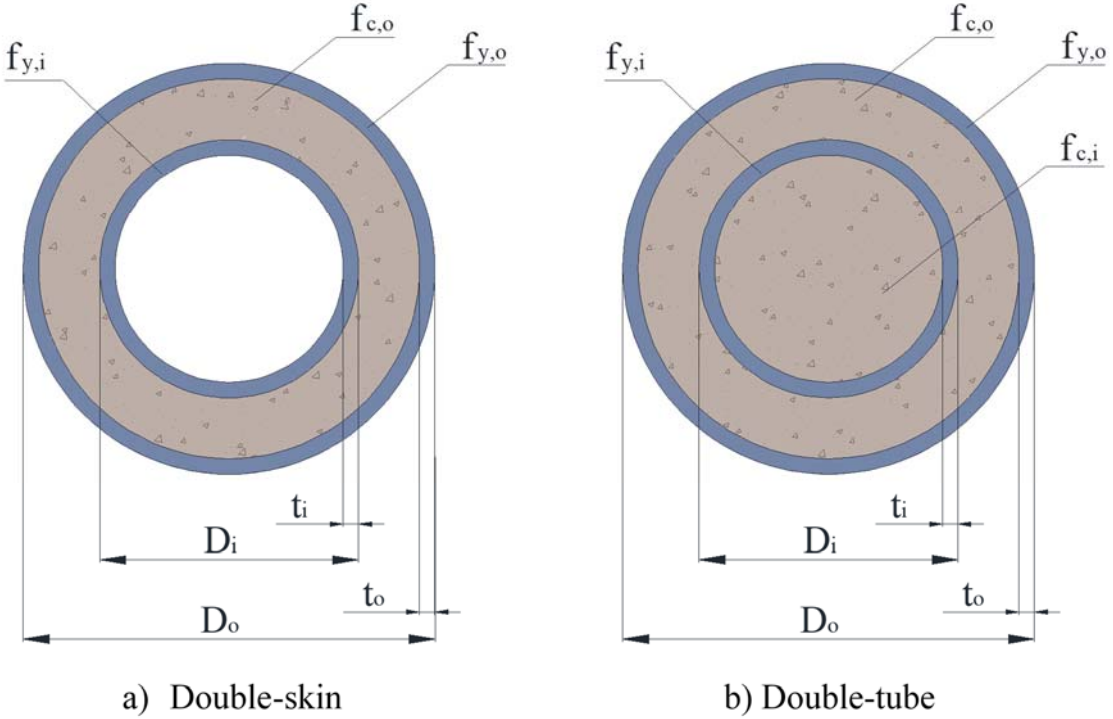


Fig. 1. CFDSST Sections.

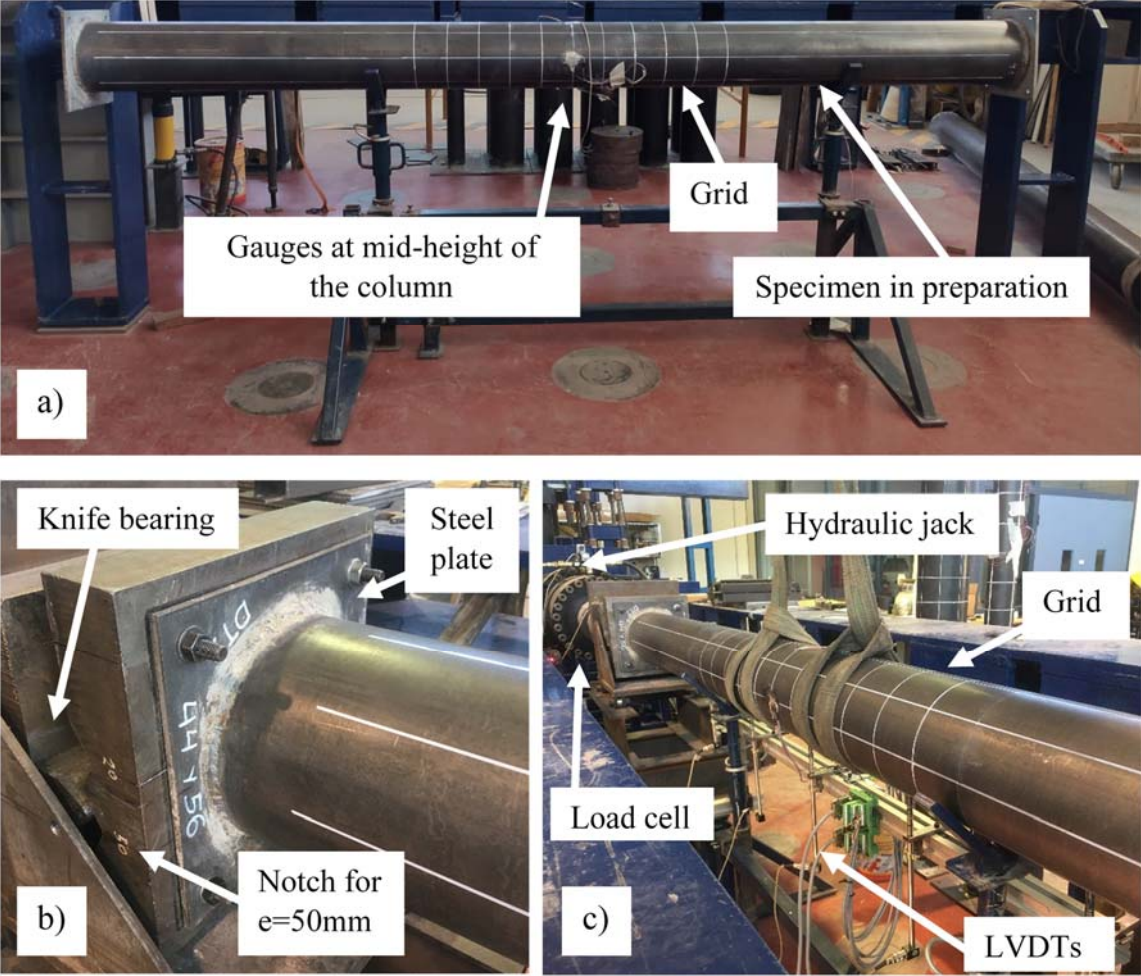


Fig. 2. a) Specimen in preparation; b) Detail of one of the ends; c) Specimen positioned in the horizontal frame.

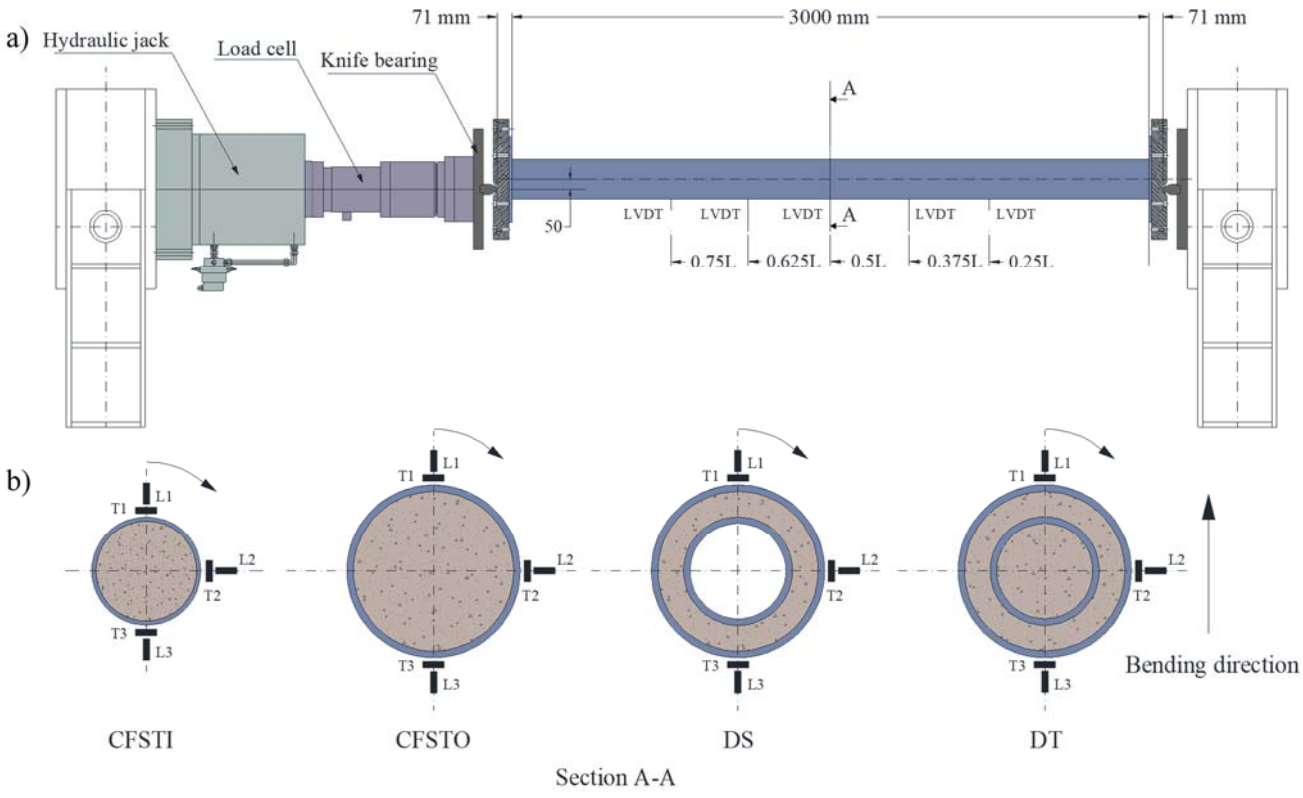


Fig. 3. a) Schematic of test setup; b) Location of strain gauges.

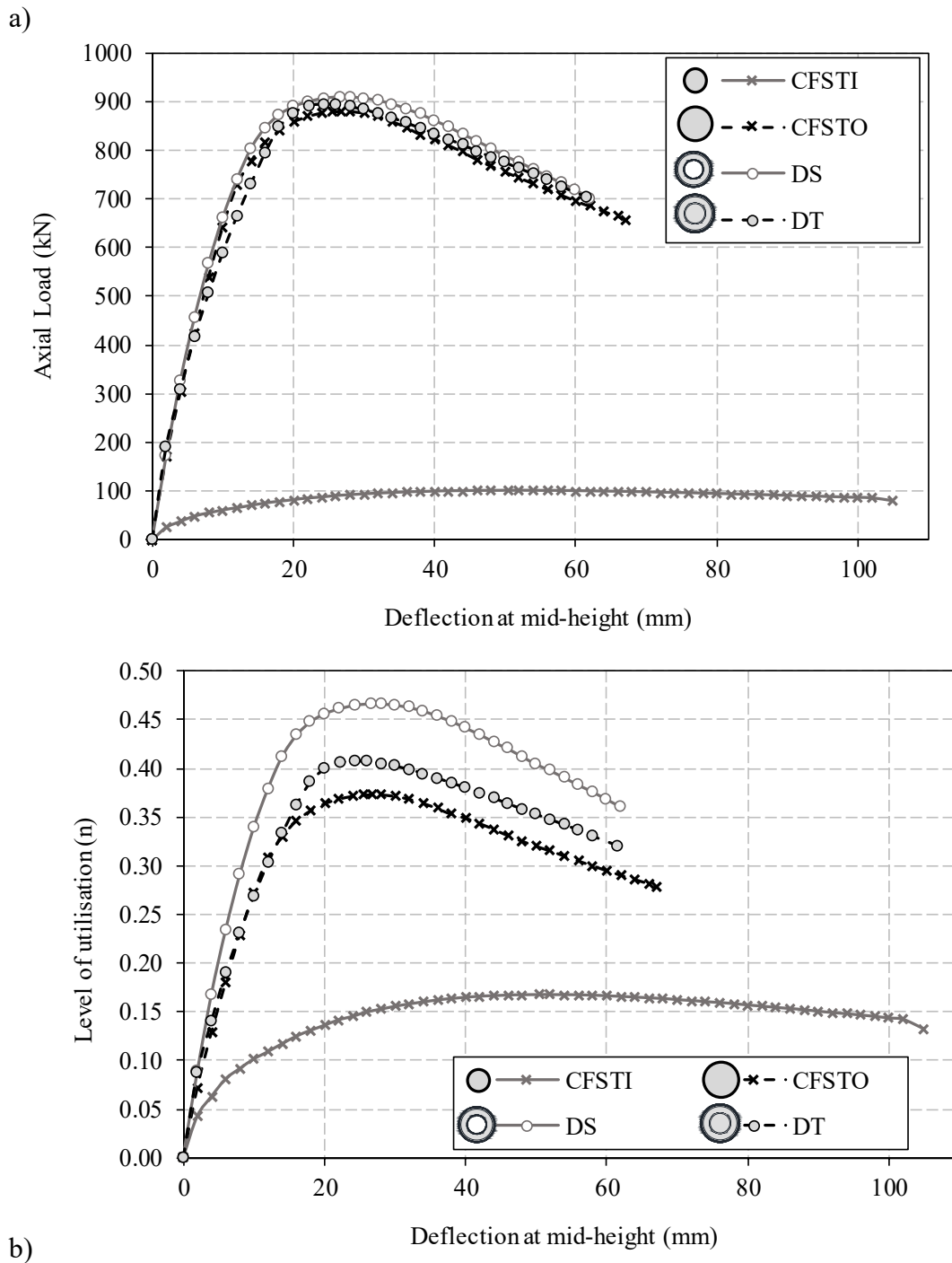


Fig. 4. a) Load versus deflection at mid-height; b) Level of utilisation versus deflection at mid-height.



Fig. 5. Columns after test.

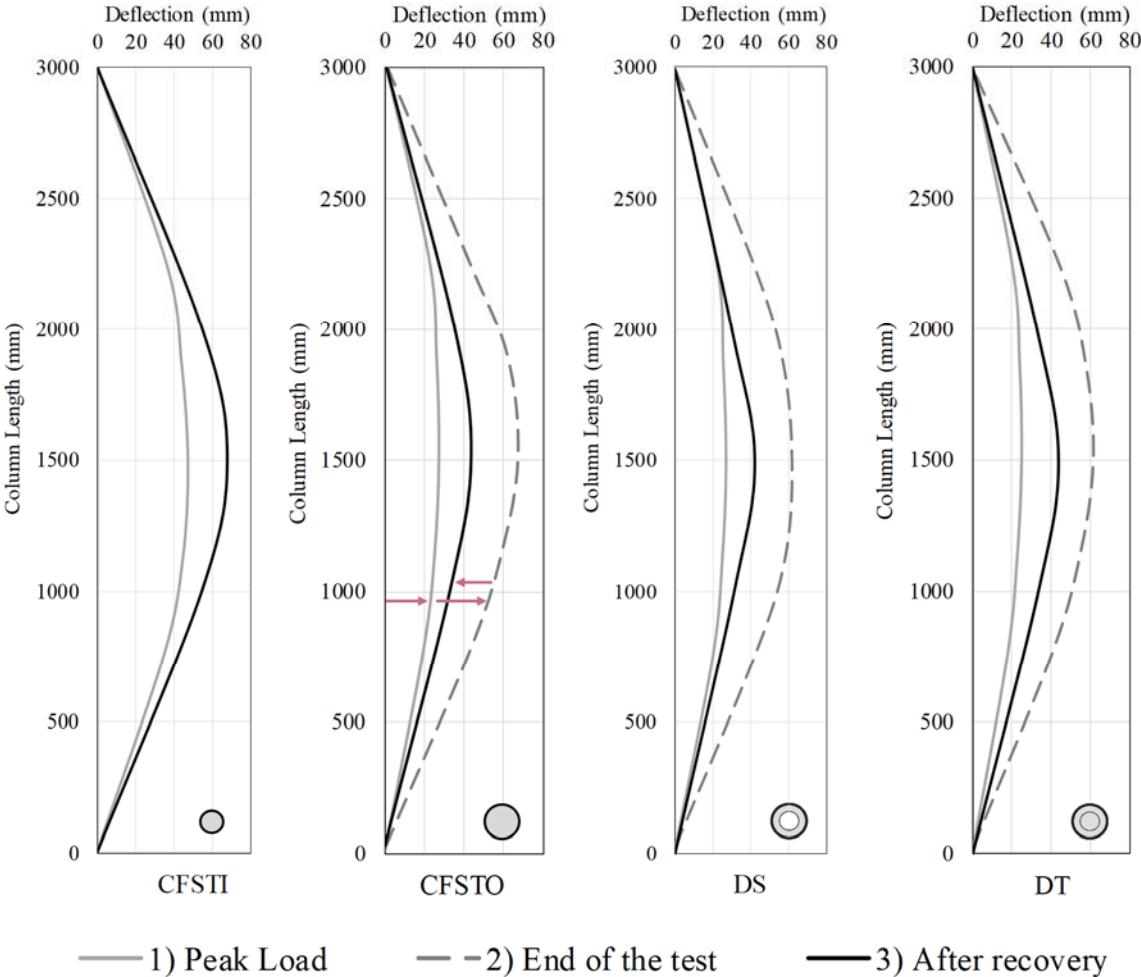


Fig. 6. Deflection of the columns at different moments.

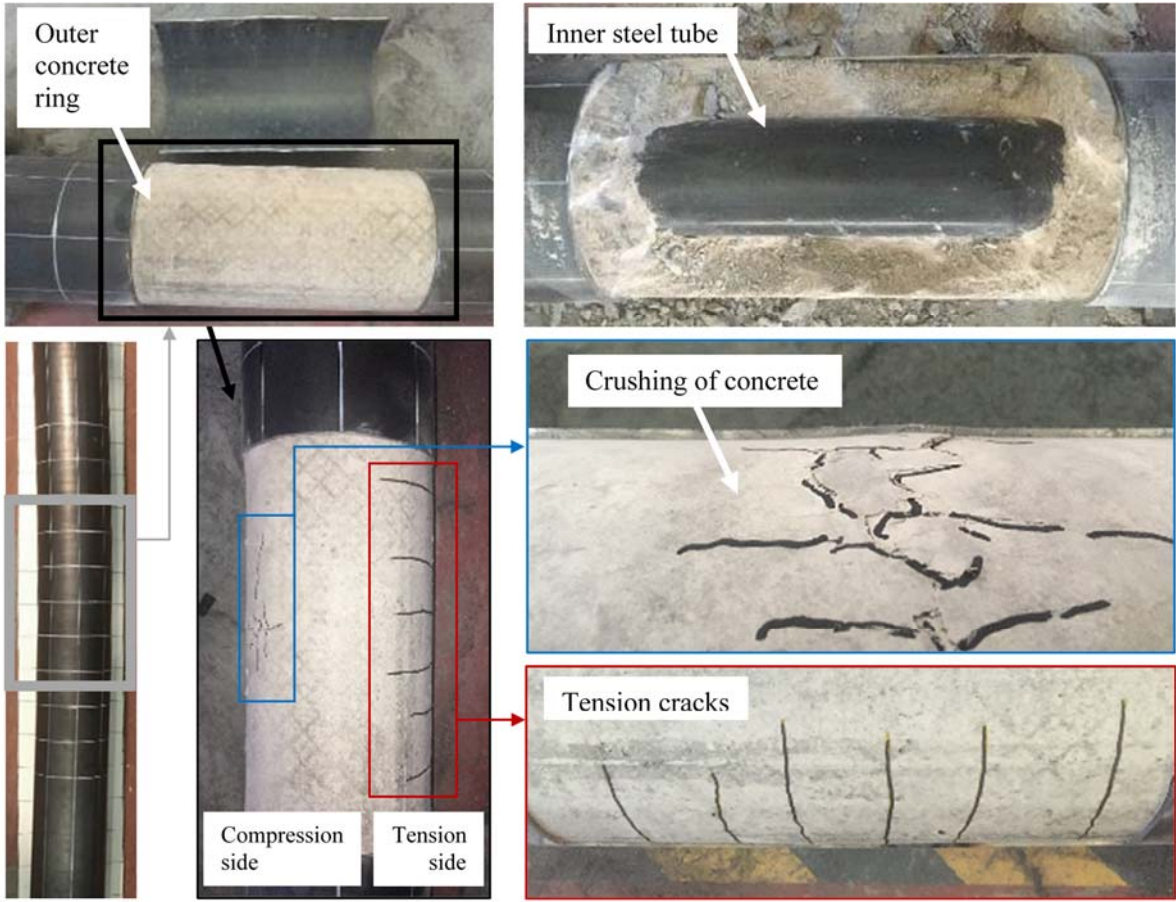


Fig. 7. Analysis of specimen DS after test.

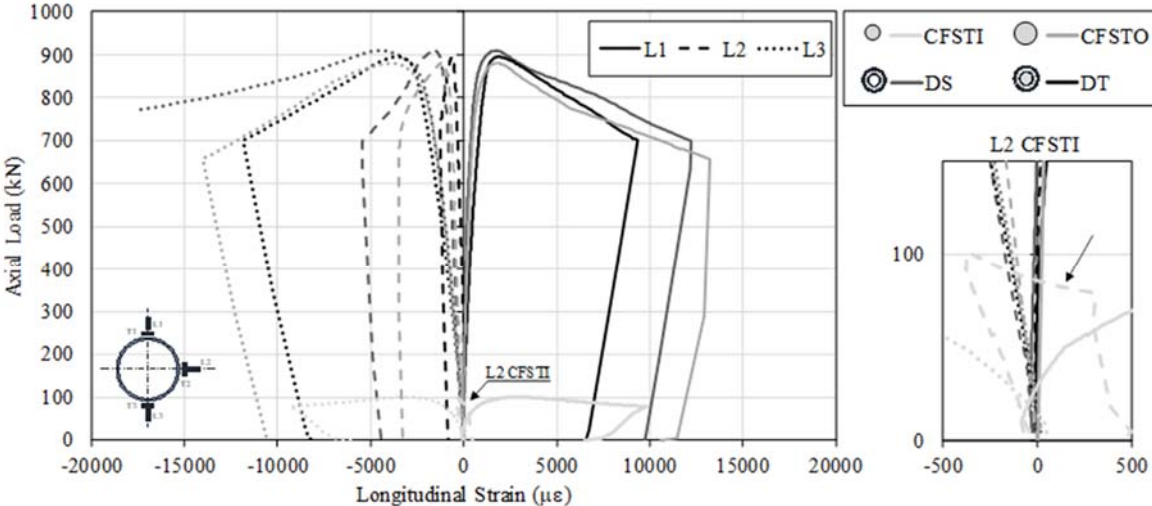


Fig. 8. Axial load versus longitudinal strain, ϵ_L .

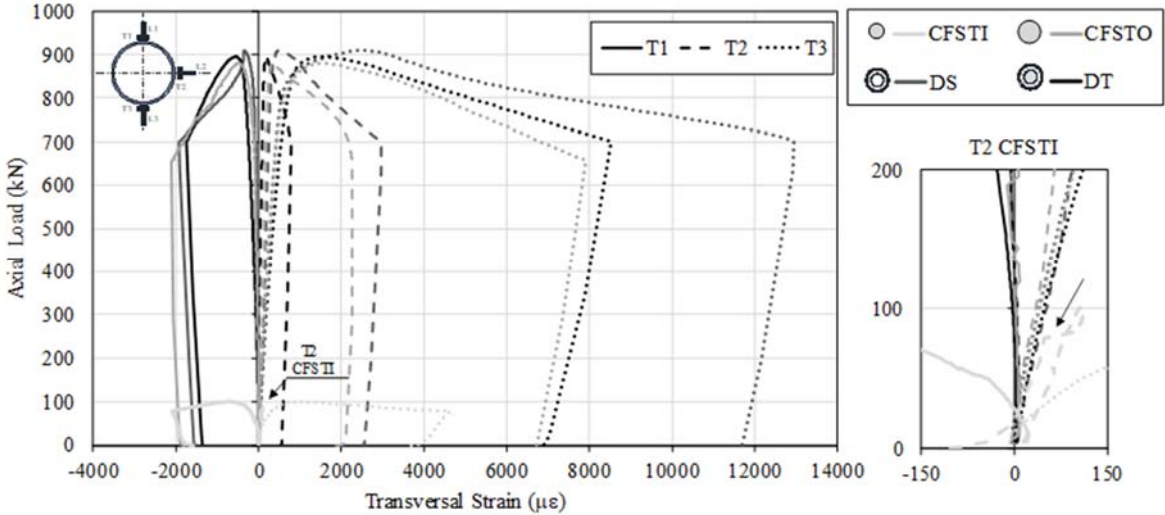


Fig. 9. Axial load versus transversal strain, ϵ_T .

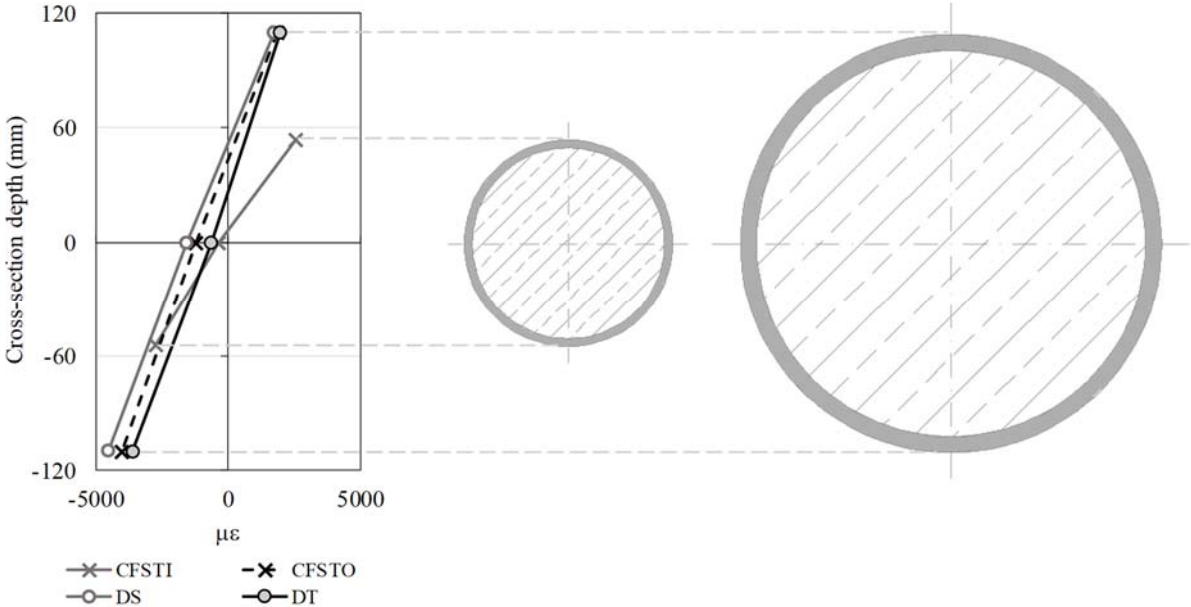


Fig. 10. Deformation of the cross-section at mid-height of the column.

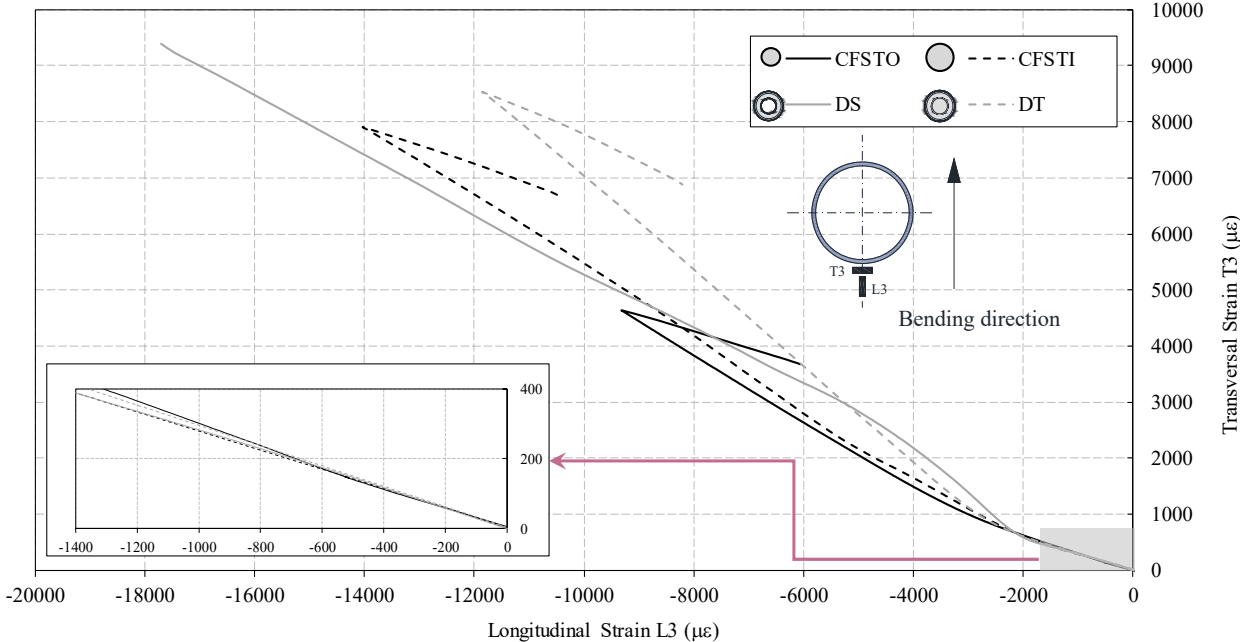


Fig. 11. Longitudinal strain versus transversal strain for gauge 3.

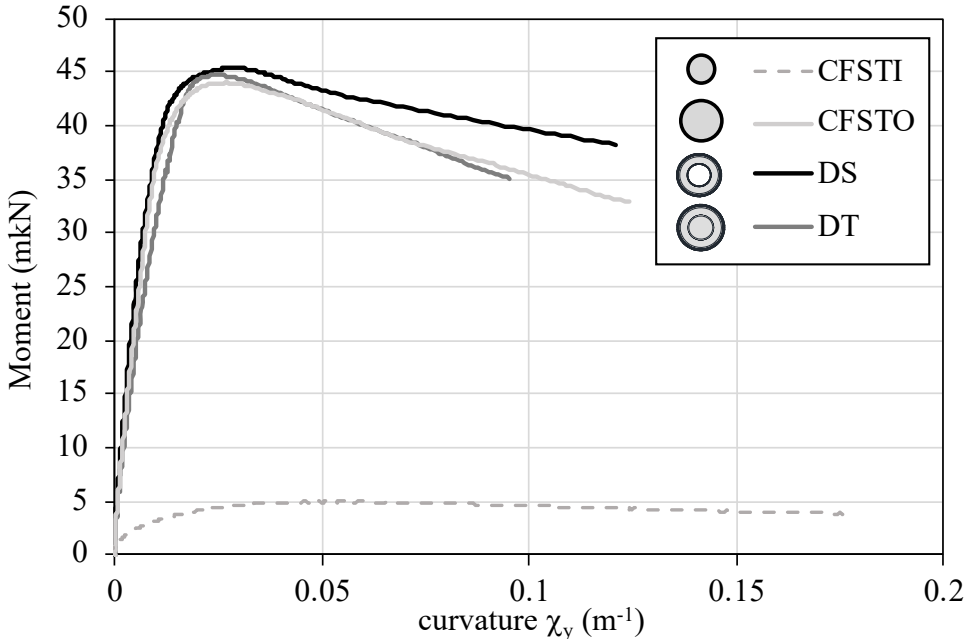


Fig. 12. $M_z-\chi_y$ curves from tests.

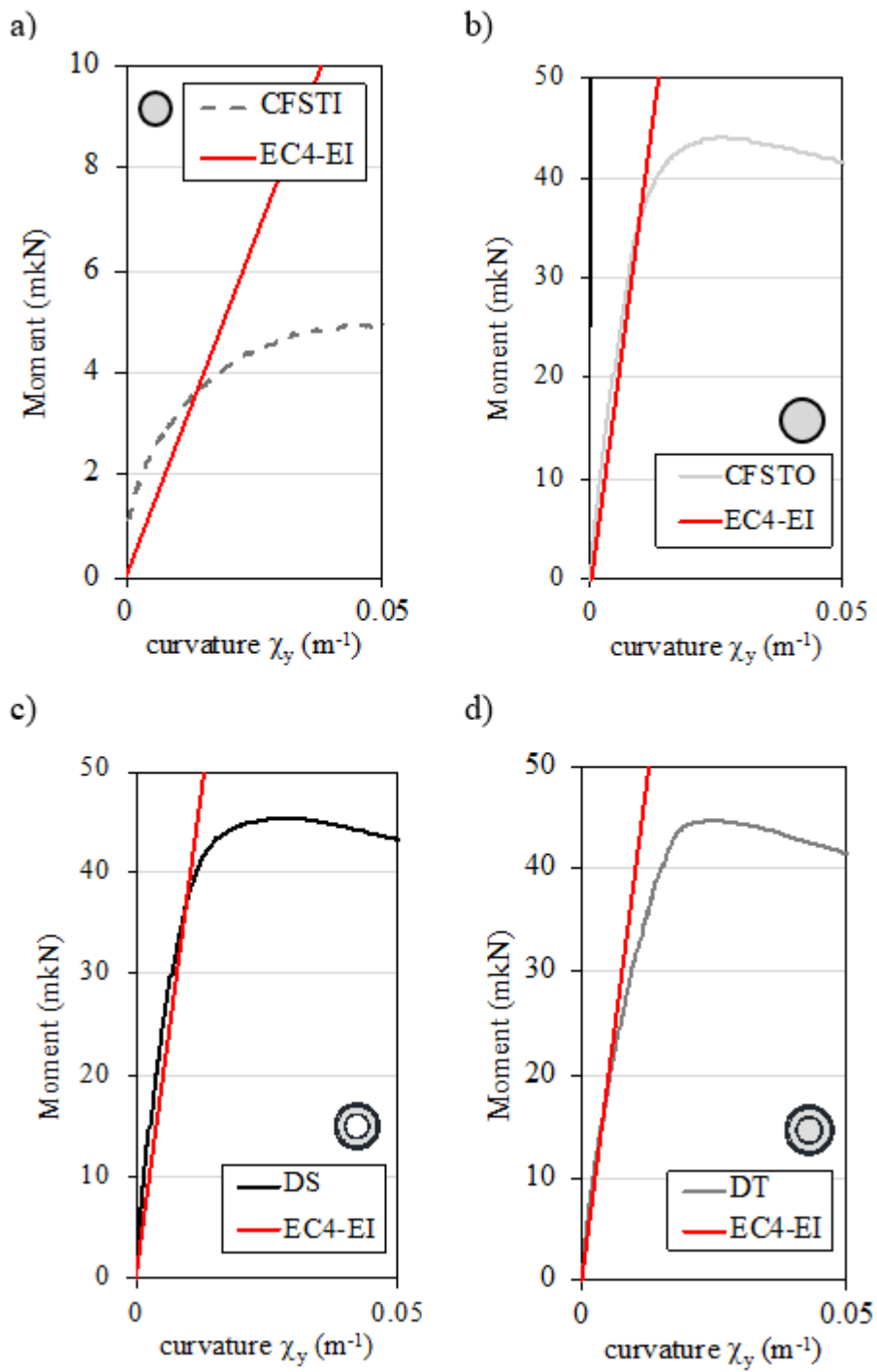
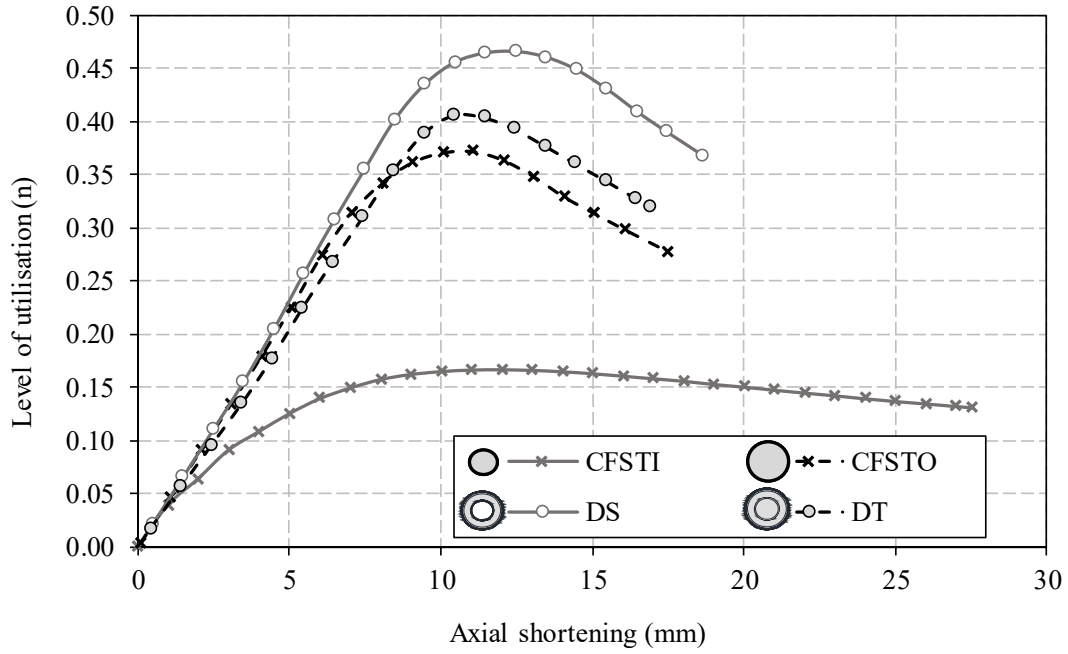


Fig. 13. Stiffness comparison: Tests versus EC4 formula.

a)



b)

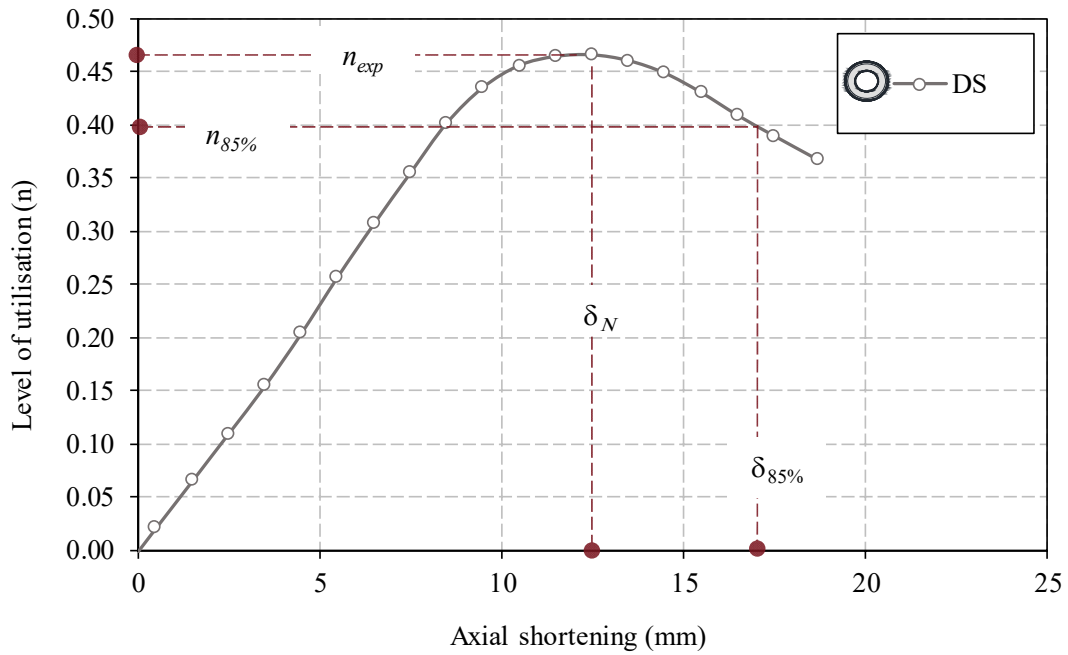


Fig. 14. a) Load versus axial shortening; b) Determination of ductility for specimen DS.

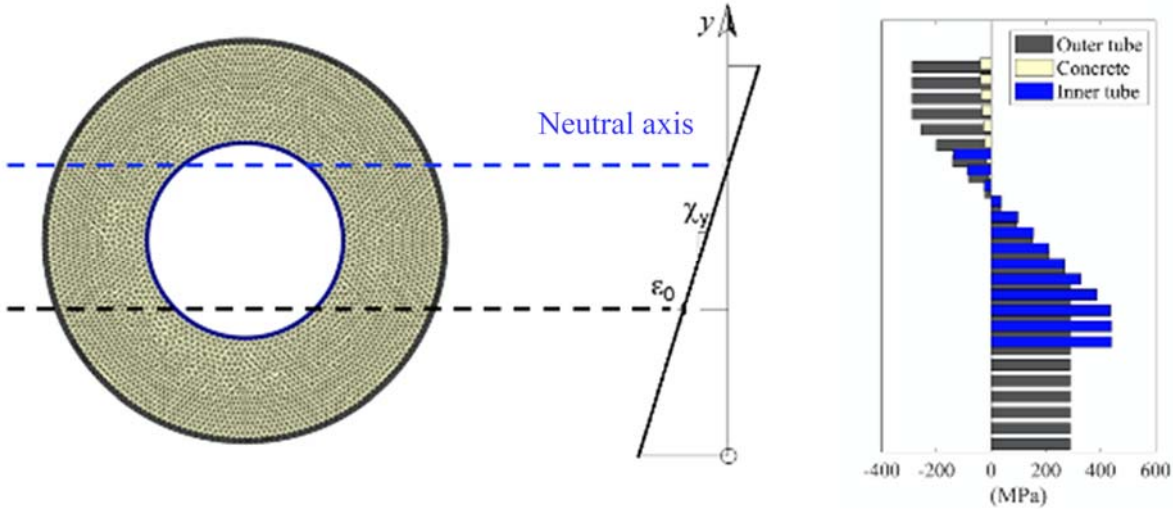


Fig. 15. DS cell discretization and strain distribution.

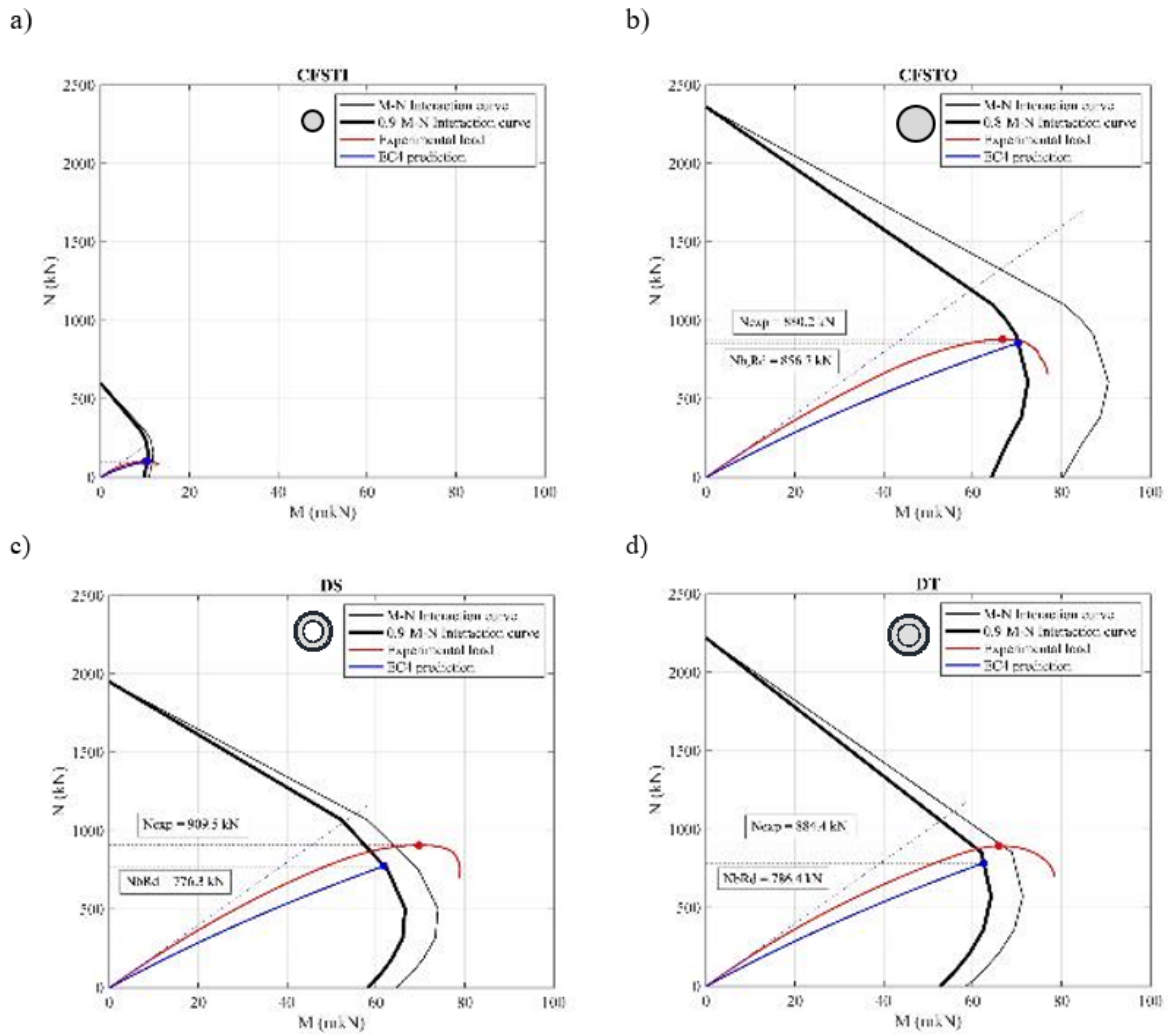


Fig. 16. M_2 - N Interaction curves. a) CFSTI; b) CFSTO; c) DS; d) DT.

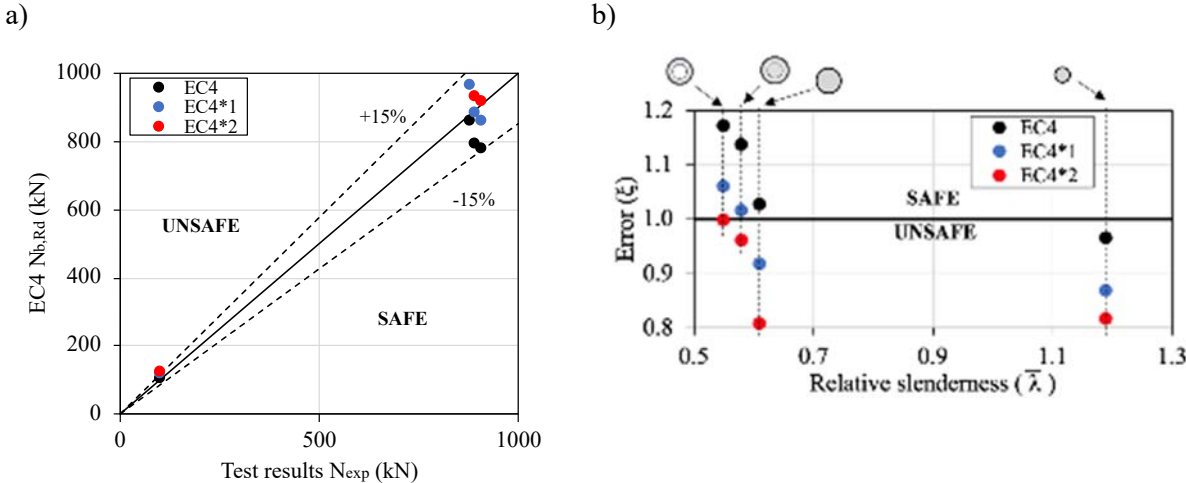


Fig. 17. a) Tests results versus EN1994-1-1 predictions; b) Calculated errors.

Table 1. Details of the specimens

ID	D_o (mm)	t_o (mm)	$f_{y,o}$ (MPa)	$f_{c,o}$ (MPa)	D_i (mm)	t_i (mm)	$N_{pl,Rd}$ (kN)	$f_{y,i}$ (MPa)	$f_{c,i}$ (MPa)	$\bar{\lambda}$	ψ
CFSTI	-	-	-	-	108	2	601.5	387.40	40.43	1.19	-
CFSTO	219.1	3	452.00	40.43	-	-	2362.5	-	40.43	0.61	-
DS	219.1	3	288.04	40.43	108	2	2199.6	439.82	40.43	0.55	0.51
DT	219.1	3	241.35	40.43	108	2	1951.2	472.00	40.43	0.58	0.51

Table 2. Test results

ID	N_{exp} (kN)	N_{end} (kN)	n_{exp}	Δ_N (mm)	Δ_{end} (mm)	$\Delta_{recovery}$ (mm)
CFSTI	100.6	78.9	0.167	47.0	-	68
CFSTO	880.2	656.7	0.373	27.4	67.1	43.5
DS	909.5	702.0	0.466	26.9	62.0	42
DT	894.4	703.3	0.406	24.9	61.6	44

Table 3. Parameters

ID	N_{exp} (kN)	$N_{85\%}$ (kN)	n_{exp}	$n_{85\%}$	δ_N (mm)	$\delta_{85\%}$ (mm)	DI	$CSCR$
CFSTI	100.6	84.6	0.167	0.142	11.32	23.14	2.05	-
CFSTO	880.2	748.3	0.373	0.317	11.06	14.88	1.35	-
DS	909.5	772.5	0.466	0.396	12.47	17.13	1.37	1.25
DT	894.4	759.8	0.406	0.346	10.43	15.35	1.47	1.08

Table 4. EN1994-1-1 predictions and errors

ID	$N_{pl,Rd}$ (kN)	Experimental		EC4		EC4 ^{*1}		EC4 ^{*2}	
		N_{exp} (kN)	$N_{b,Rd}$ (kN)	ξ	$N_{b,Rd}$ (kN)	ξ	$N_{b,Rd}$ (kN)	ξ	
CFSTI	601.5	100.6	104.1	0.97	115.6	0.87	123.1	0.82	
CFSTO	2362.5	880.2	856.7	1.03	958.3	0.92	1087.7	0.81	
DS	2199.6	909.5	776.3	1.17	857.6	1.06	910.7	1.00	
DT	1951.2	894.4	786.4	1.14	880.0	1.02	928.9	0.96	
Mean				1.08		0.97		0.90	
Standard deviation				0.10		0.09		0.10	
Coefficient of Variation (COV)				0.09		0.09		0.11	

EC4^{*1} does not take into account the member imperfection

EC4^{*2} does not take into account the member imperfection and α_M coefficient ($\alpha_M=1$)

LIST OF FIGURE CAPTIONS

Fig. 1. CFDST Sections.

Fig. 2. a) Specimen in preparation; b) Detail of one of the ends; c) Specimen positioned in the horizontal frame.

Fig. 3. a) Schematic of test setup; b) Location of strain gauges.

Fig. 4. a) Load versus deflection at mid-height; b) Level of utilisation versus deflection at mid-height.

Columns after test.

Fig. 6. Deflection of the columns at different moments.

Fig. 7. Analysis of specimen DS after test.

Fig. 8. Axial load versus longitudinal strain, ϵ_L .

Fig. 9. Axial load versus transversal strain, ϵ_T .

Fig. 10. Deformation of the cross-section at mid-height of the column.

Fig. 11. Longitudinal strain versus transversal strain for gauge 3.

Fig. 12. $M_z-\chi_y$ curves from tests.

Fig. 13. Stiffness comparison: Tests versus EC4 formula.

Fig. 14. a) Load versus axial shortening; b) Determination of ductility for specimen DS.

Fig. 15. DS cell discretization and strain distribution.

0.

Fig. 17. a) Tests results versus EN1994-1-1 predictions; b) Calculated errors.

LIST OF TABLE CAPTIONS

Table 1. Details of the specimens

Table 2. Test results

Table 3. Parameters

Table 4. EN1994-1-1 predictions and errors